JOURNAL OF INTEGRAL EQUATIONS AND APPLICATIONS
Vol. , No. , YEAR
https://doi.org/jie.YEAR..PAGE

UNIFORMLY CONVERGENT NUMERICAL METHOD FOR A SYSTEM OF VOLTERRA INTEGRO-DIFFERENTIAL EQUATIONS EXHIBITING BOUNDARY LAYERS

A. PANDA AND J. MOHAPATRA

ABSTRACT. In this article, we study a system of singularly perturbed non-linear Volterra integro-differential equations. The leading term of each equation is multiplied by a small positive parameter whose magnitude may vary. The presence of these parameters creates interacting and overlapping boundary layers in the solution. To resolve the issue of boundary layers, the piecewise uniform Shishkin mesh and the Bakhvalov-Shishkin mesh is formed. On these meshes, an upwind scheme for the derivative part along with the left rectangular rule for the integral part proves to be almost first order convergent uniformly in both parameters. Further, a post-processing technique is employed that improves the order of accuracy to second order. At the end, the theoretical findings are supported by a few numerical computations.

A widely recognized approach for modeling various physical problems involves using systems of Volterra integro-differential equations (VIDEs). These system of equations were formulated for describing the activity of interacting inhibitory and excitatory neurons by the Wilson-Cowan model [20]. Its use in constructing boundary value problems for scattering [3], electrostatics [13], and fluid dynamics [19] has historically been quite popular among mathematicians and physicists. The VIDEs exhibit boundary layers when a small positive quantity is multiplied to the highest order derivative term and are referred to as singularly perturbed Volterra integro-differential equations (SPVIDEs) [12].

Due to the existence of boundary layers, whose width is dependent on the perturbation parameter, the conventional numerical approaches for single (uncoupled) singularly perturbed problems applied on uniform meshes are insufficient [16]. These layers are not resolved unless an unreasonably high number of mesh points is employed. The analytical techniques based on the generalized power series method [6], additive decomposition method [2] are studied for solving the singularly perturbed differential equation. The problem gets more challenging for coupled system. Since the perturbation parameters linked to each equation are different from one another, the solution to any particular equation in the system includes a sub layer for each of the parameters in the overall problem. Hence, developing numerical methods and doing their analysis become quite complex [14].

For the systems of linear VIDEs, Berenguer et al. in [1] solved a system of VIDEs using the approximation methods, Liang and Brunner in [9] suggested the collocation approaches. Also, in the context of uncoupled SPVIDEs, numerous reliable techniques are developed. (One may see [5, 15, 18]). But very few works are done related to the coupled SPVIDEs. In [7], using a uniform

Corresponding author.

2020 *Mathematics Subject Classification.* 65L11, 65L20, 34A34.

Key words and phrases. Volterra integro-differential equation, Singular perturbation, System of equations, Convergence analysis.

grid, Kauthen constructed the implicit Volterra Runge Kutta methods for a system of SPVIDEs with a single perturbation parameter. Recently, Liang et al. [10] studied a posteriori error estimation for a system of SPVIDEs and obtained first order convergence. However, to the best of our knowledge, there are no numerical algorithms for a system of SPVIDEs that can converge at second order. In this work, our main intention is to develop an efficient, global second order accurate and parameter-uniform numerical approximation for a system of SPVIDEs.

Consider the following one-dimensional system of integro-differential equations.

$$(1)\qquad L_\varepsilon \mathbf{u}(t) = \begin{cases} \varepsilon_r u_r'(t) + \sum_{j=1}^{2} a_{rj}(t)u_j(t) + \sum_{j=1}^{2}\int_0^t \mathcal{K}_{rj}(t,s)u_j(s)ds = f_r(t), \;\; r=1,2, \\ u_1(0)=\eta_1, \quad u_2(0)=\eta_2. \end{cases}$$

Rewriting the above equations for $t \in \Omega := (0,1)$ we have:

$$(2)\qquad L_\varepsilon \mathbf{u} := \varepsilon \mathbf{u}' + A\mathbf{u} + \int_0^t \mathcal{K}(t,s)\mathbf{u}(s)ds = f, \;\; \mathbf{u}(0)=\eta,$$

where the unknown solution is denoted by $\mathbf{u} = (u_1,u_2)^T$, $f=(f_1,f_2)^T$ and $\eta = (\eta_1,\eta_2)^T$; $A = a_{rj}(t)$, $\mathcal{K} = \mathcal{K}_{rj}$ is a 2×2 matrix and $\varepsilon = \mathrm{diag}(\varepsilon_1,\varepsilon_2)$ is a diagonal matrix with small perturbation parameters. For simplicity, we consider $0<\varepsilon_1 \le \varepsilon_2 \ll 1$, the other case when $\varepsilon_2 \le \varepsilon_1$ can also be solved in a similar way. The above equations satisfy the following inequalities:

$$(3)\qquad a_{ij}(t) \ge \alpha_{ij} > 0,\; a_{ij} \le 0,\; i \ne j, \text{ for } t \in [0,1];$$

$$(4)\qquad \gamma_i = \max_{t\in[0,1]} |a_{ij}(t)|, \;\; i \ne j;$$

$$(5)\qquad \widetilde{W}_i = \max_{t,s\in[0,1]} |\mathcal{K}_{ii}(t,s)|, \;\; W_i = \max_{t,s\in[0,1]} |\mathcal{K}_{ij}(t,s)|, \;\; i\ne j.$$

The functions $a_{rj}, f_r, \mathcal{K}_{rj} \in C(\overline{\Omega})$ and $\alpha = \min(\alpha_1,\alpha_2)$. The model (1) has a unique solution with all the above conditions and also possesses overlapping left end boundary layers at $t=0$ as $\varepsilon \to 0$. The main advantage of our work is to formulate a numerical scheme that not only gives a better order of convergence for the considered model problem, but also improve the accuracy of results as the mesh is refined in comparison to [10].

The organizational structure of the article is as follows: Section 1 proves the bounds of the exact solution followed by the formation of meshes and numerical discretization in Section 2. The analysis of the upwind scheme is carried out in Section 3. Section 4 implements a post-processing technique along with their global error bounds. Numerical experiments and comparison of results are shown in Section 5 for the validation of theoretical findings. Finally, the article is summarized in Section 6. Throughout the article, for any function $f(t)$, we set $f_i = f(t_i)$ and let $C>0$ denotes a generic constant independent of N, ε_1 and ε_2. The notations $\mathscr{C}^k(\overline{\Omega})$ and $\mathscr{C}^k(\Omega)$ denotes k times continuously differentiable function in the respective domains. The maximum norm is defined by $||z|| = \max\{\|z_1\|, \|z_2\|\}$ and for any mesh function, $Z = \{(Z_1(t_i), Z_2(t_i))^T\}_{i=0}^N$, we define $||Z||_\infty = \max\{\|Z_1\|_\infty, \|Z_2\|_\infty\}$.

1. Analytical properties

In this section, we describe the properties of the exact solution. The stability of the solution is established which is later used in the error analysis.

Lemma 1.1. *Under the conditions (3)-(5), the solution of problem (1) satisfies the following estimate:*

$$\|\mathbf{u}\| \le C(\|\eta\| + \|f\|).$$

Proof. The first equation of (1) can be rewritten as:

$$\varepsilon_1 u_1'(t) + a_{11}(t)u_1(t) + \int_0^t \mathcal{K}_{11}(t,s)u_1(s)ds = F_1(t), \tag{6}$$

where

$$F_1(t) = f_1(t) - a_{12}(t)u_2(t) - \int_0^t \mathcal{K}_{12}(t,s)u_2(s)ds.$$

Similar to Lemma 2.1 in [4], we have,

$$\begin{aligned} u_1(t) = |\eta_1| \exp\left(\frac{-\alpha_1 t}{\varepsilon_1}\right) &+ \frac{1}{\varepsilon_1}\int_0^t F_1(s)\exp\left(-\frac{1}{\varepsilon_1}\int_s^t a_{11}(t)dt\right)ds \\ &- \frac{1}{\varepsilon_1}\int_0^t \left[\int_0^s \mathcal{K}_{11}(s,\xi)u_1(\xi)d\xi\right]\exp\left(-\frac{1}{\varepsilon_1}\int_s^t a_{11}(t)dt\right)ds \end{aligned}$$

It follows from (3)-(5) that:

$$\begin{aligned} |u_1(t)| = |\eta_1|\exp\left(-\frac{\alpha_1 t}{\varepsilon_1}\right) &+ \frac{1}{\varepsilon_1}\int_0^t |F_1(s)|\exp\left(-\frac{\alpha_1(t-s)}{\varepsilon_1}\right)ds \\ &+ \frac{1}{\varepsilon_1}\int_0^t \left[\int_0^s [\mathcal{K}_{11}(s,\xi)|u_1|(\xi)]d\xi\right]\exp\left(-\frac{\alpha_1(t-\xi)}{\varepsilon_1}\right)ds \\ \le |\eta_1| + \frac{1}{\varepsilon_1}\int &\left| f_1(s) - a_{12}(s)u_2(s) - \int_0^s \mathcal{K}_{12}(s,\xi)u_2(\xi)d\xi\right|\exp\left(-\frac{\alpha_1(t-s)}{\varepsilon_1}\right)ds \\ &+ \frac{\widetilde{W_1}}{\alpha_1}\left(1-\exp\left(-\frac{\alpha_1 t}{\varepsilon_1}\right)\right)\int_0^t |u_1(s)|ds \\ \le |\eta_1| + \frac{|f_1|}{\alpha_1} &+ \frac{(\gamma_1 + W_1)}{\alpha_1}\|u_2\| + \frac{(\widetilde{W}_1)}{\alpha_1}\int_0^t |u_1(s)|ds. \end{aligned}$$

Employing the Gronwall's inequality, the above expression becomes:

$$|u_1(t)| = \left[|\eta_1| + \frac{|f_1|}{\alpha_1} + \frac{(\gamma_1 + W_1)}{\alpha_1}\|u_2\|\right]\exp(\alpha_1^{-1}\widetilde{W_1}t). \tag{7}$$

In a similar way, for the second equation of (1), we get:

$$|u_2(t)| = \left[|\eta_2| + \frac{|f_2|}{\alpha_1} + \frac{(\gamma_2 + W_2)}{\alpha_1}\|u_1\|\right]\exp(\alpha_2^{-1}\widetilde{W_2}t). \tag{8}$$

Finally obtaining the bounds, we have

$$M\begin{pmatrix}\|u_1\| \\ \|u_2\|\end{pmatrix} \le C\begin{pmatrix}|\eta_1| + \|f_1\| \\ |\eta_2| + \|f_2\|\end{pmatrix}, \tag{9}$$

where

$$M = \begin{pmatrix} 1 & -\dfrac{\gamma_1 + W_1}{\alpha_1} \exp(\alpha_1^{-1}\widetilde{W}_1) \\ -\dfrac{\gamma_2 + W_2}{\alpha_2} \exp(\alpha_2^{-1}\widetilde{W}_2) & 1 \end{pmatrix}.$$

We know 'M' is a monotone matrix iff $\mathrm{M}^{-1} \geq 0$. Now, in the above expression, assuming, M is inverse monotone, thus $M^{-1} > 0$, which completes the proof. □

Lemma 1.2. *Let $\mathbf{u}(t) \in \mathscr{C}^2(\Omega)$ be the solution of (1), then the k^{th} derivative of the exact solution satisfies the following inequality:*

$$|\mathbf{u}^k(t)| \leq C\left(1 + \frac{1}{\varepsilon^k} e^{-\alpha t/\varepsilon}\right), \ \textit{for} \ k = 1, 2.$$

Proof. Differentiating $L_\varepsilon \mathbf{u} = \varepsilon \mathbf{u}' + A\mathbf{u} + \int_0^t \mathcal{K}(t,s)\mathbf{u}(s)ds = f$, we get

$$L_\varepsilon \mathbf{u}' = f' - A'\mathbf{u} - \mathcal{K}(t,t)\mathbf{u}(t) + \mathcal{K}(t,0)\mathbf{u}(0) - \int_0^t \frac{\partial}{\partial t}\Big(\mathcal{K}(t,s)\mathbf{u}(s)\Big) ds.$$

Now, using Lemma 1.1, denoting the bound on $\mathbf{u}$ and considering the fact that kernel $\mathcal{K}$ is a bounded function, we get $|\mathbf{u}'(t)| \leq \dfrac{C}{\varepsilon} \exp\left(\dfrac{-\alpha t}{\varepsilon}\right) + C$. Similarly, the bounds for $\mathbf{u}''(t)$ can be obtained using induction. □

2. Mesh and discretization

In this section, first we generate the non-uniform meshes and then discretize (1) using appropriate schemes. In the case of left boundary layer, we divide the domain $[0,1]$ into two sub-intervals corresponding to the region where the solution is smooth and to the boundary layers at $t = 0$. When $0 < \varepsilon_1 \leq \varepsilon_2 \ll 1$, the solution to (1) has overlapping boundary layers at $t = 0$. This necessitates the construction of a mesh that is uniform on each sub-intervals $[0, \tau_{\varepsilon_1}]$, $[\tau_{\varepsilon_1}, \tau_{\varepsilon_2}]$ and $[\tau_{\varepsilon_2}, 1]$. On the main sub-interval, where the smooth solution exists the mesh is coarse, else on the other two intervals the mesh is finer. For the construction of the Shishkin mesh (S mesh), first we define the transition points as $\tau_{\varepsilon_2} = \min\left(\dfrac{1}{2}, \dfrac{2\varepsilon_2}{\alpha}\ln N\right)$, $\tau_{\varepsilon_1} = \min\left(\dfrac{\tau_{\varepsilon_2}}{2}, \dfrac{2\varepsilon_1}{\alpha}\ln N\right)$ and $\alpha = \min(\alpha_1, \alpha_2)$. Then, a piecewise uniform S mesh is constructed by subdividing $[\tau_{\varepsilon_2}, 1]$ into $\dfrac{N}{2}$ mesh intervals and subdivide the other two portions into $\dfrac{N}{4}$ mesh intervals. When $\tau_{\varepsilon_1} = \dfrac{\tau_{\varepsilon_2}}{2}$, then $\varepsilon_2 = O(\varepsilon_1)$, and the results can be easily obtained. Therefore, we only consider the case where $\tau_{\varepsilon_1} < \dfrac{\tau_{\varepsilon_2}}{2}$. The mesh Ω_N is generated as follows

$$t_i = \begin{cases} \dfrac{4\tau_{\varepsilon_1} i}{N}, & 0 \le i \le \dfrac{N}{4} \\ \tau_{\varepsilon_1} + \left(i - \dfrac{N}{4}\right) \dfrac{4(\tau_{\varepsilon_1} - \tau_{\varepsilon_2})}{N}, & \dfrac{N}{4} < i \le \dfrac{N}{2}, \\ \tau_{\varepsilon_2} + \left(i - \dfrac{N}{2}\right) \dfrac{2(1-\tau_{\varepsilon_2})}{N}, & \dfrac{N}{2} < i \le N. \end{cases} \tag{10}$$

The Shishkin mesh (S mesh) is generated using the mesh function $\Psi(t) = 2t\ln N$. Similarly, we can generate the Bakhvalov-Shishkin mesh (B-S mesh) using the mesh generating function $\Psi(t) = -\ln[1-2(1-N^{-1})t]$. The function $\Psi(t)$ is a monotonically decreasing function satisfying $\Psi(0) = 1$, and $\Psi\left(\dfrac{1}{2}\right) = \ln N$. The following discrete scheme is proposed for solving (1) for $i = 1,\dots,N$:

$$(L_r^N U_r{}^N)_i = \begin{cases} \varepsilon_r (D^- U^N{}_r)_i + \displaystyle\sum_{w=1}^{2} a_{rw}(t_i) U_{wi}^N + \sum_{w=1}^{2}\sum_{j=0}^{i-1} \mathcal{K}_{rw}(t_i,t_j) U_{wj}^N h_j = f_r(t_i), \\ (U_r^N)_0 = \eta_r, \ r = 1,2. \end{cases} \tag{11}$$

The numerical solution for t_i, $i = 1,2,\dots,N$ and system of two equations $r = 1,2$ are defined by $U_{r,i}^N$. The differential operator $D^-(U_r^N)_i = \dfrac{U_{r,i}^N - U_{r,i-1}^N}{t_i - t_{i-1}}$, is the backward Euler scheme used to approximate the first order differentials. $(U_r^N)_i$ is the discrete solution for $i = 1,2,\dots,N$ and $r = 1,2$. (r implies system of equations)

Lemma 2.1. *For a piecewise differentiable mesh generating function Ψ satisfying the condition*

$$\max_{[0,1/2]} \Psi'(x) = \max_{[0,1/2]} \frac{|\Psi'|}{\Psi} \le CN,$$

the following inequality holds:

$$\max_i \int_{x_{i-1}}^{x_i} (1+\varepsilon^{-1}\exp(-\alpha x/k\varepsilon))dx \le C\left\{\varepsilon + \left(N^{-1} + N^{-\tau/k}\right) \max_{x\in[0,1/2]} |\Psi'(x)|\right\},$$

where

$$\max_{x\in[0,1/2]} |\Psi'(x)| \le C\ln N, \quad S\ \ Mesh,$$

$$\max_{x\in[0,1/2]} |\Psi'(x)| \le C, \quad B\text{-}S\ \ Mesh.$$

3. Analysis of the scheme

In this section, the stability bounds are discussed along with a detailed analysis on the bounds of truncation error. Rewriting (11), we get

$$L^N \mathbf{U}_i^N \equiv l^N \mathbf{U}_i^N + \hat{A}(t_i)\mathbf{U}_i^N + \sum_{j=0}^{i-1} \mathcal{K}(t_i,t_j)\mathbf{U}_j^N h_j = f(t_i), \ \ 1 \le i \le N, \tag{12}$$

where

$$l^N \mathbf{U}_i^N \equiv \varepsilon D^- \mathbf{U}_i^N + A(t_i)\mathbf{U}_i^N,$$

$$\hat{A}(t_i) = \begin{pmatrix} 0 & a_{12}(t_i) + h_i \mathcal{K}_{12}(t_i,t_i) \\ a_{21}(t_i) + h_i \mathcal{K}_{21}(t_i,t_i) & 0 \end{pmatrix}$$

$$\text{and } \; A(t_i) = \begin{pmatrix} a_{11}(t_i) + h_i \mathcal{K}_{11}(t_i,t_i) & 0 \\ 0 & a_{22}(t_i) + h_i \mathcal{K}_{22}(t_i,t_i) \end{pmatrix}$$

For $r = 1,2$, we assume that there exist two constants $\widetilde{\alpha}_r$, such that:

$$\alpha_r + h_i \mathcal{K}_{rr}(t_i,t_i) \geq \widetilde{\alpha}_r > 0, \;\; 1 \leq i \leq N. \tag{13}$$

Denote $L^N \mathbf{U}_i^N = (L_1^N U_{1i}^N, L_2^N U_{2i}^N)^T$ and $l^N \mathbf{U}_i^N = (l_1^N U_{1i}^N, l_2^N U_{2i}^N)^T$. Then, under the assumptions (3), (13) and Lemma 3.1 of [8], we reach at

$$\max_{0\leq i\leq N} |U_{ri}^N| \leq |U_{r0}^N| + \widetilde{\alpha}_r^{-1} \max_{1\leq i\leq N} \left| l_r^N U_{ri}^N \right|, \;\; r = 1,2. \tag{14}$$

Now, to derive the stability bounds of the discrete scheme, we have the following lemma.

Lemma 3.1. *Under the conditions (3) and (13), for the numerical solution $\mathbf{U}^N = (U_1^N, U_2^N)^T$ of (11), we have:*

$$\|\mathbf{U}^N\|_\infty \leq C(\|\eta\| + \|f\|). \tag{15}$$

Proof. Consider the first equation from (12) and using $\overline{\mathcal{K}}_1 = \max |\mathcal{K}_{1j}|, \; j = 1,2$, we have:

$$|l_1^N U_{1i}^N| = \left| L_1^N U_{1i}^N - a_{12}(t_i) U_{2i}^N - \sum_{j=0}^{i-1} \mathcal{K}_{12}(t_i,t_j) U_{2j}^N h_j - \sum_{j=0}^{i-1} \mathcal{K}_{11}(t_i,t_j) U_{1j}^N h_j \right|$$

$$\leq |f_1(t_i)| + C \max_{0\leq i\leq N} |U_{2i}^N| + \overline{\mathcal{K}}_1 \sum_{j=1}^{i-1} h_j |U_{1j}^N|.$$

From (14), one can write

$$\max_{0\leq i\leq N} |U_{1i}^N| \leq |\eta_1| + C\left(\|f_1(t)\|_\infty + \max_{0\leq i\leq N} |U_{2i}^N| + \sum_{j=1}^{i-1} h_j |U_{1j}^N| \right). \tag{16}$$

Applying the discrete Gronwall inequality to (16) yields:

$$\max_{0\leq i\leq N} |U_{1i}^N| \leq C\left(|\eta_1| \left[\|f_1(t)\|_\infty + \max_{0\leq i\leq N} |U_{2i}^N| \right] \right). \tag{17}$$

Similarly, we have

$$\max_{0\leq i\leq N} |U_{2i}^N| \leq C\left(|\eta_2| \left[\|f_2(t)\|_\infty + \max_{0\leq i\leq N} |U_{1i}^N| \right] \right). \tag{18}$$

Combining (17) and (18), we obtain:

$$\overline{M} \|\mathbf{U}^N\|_\infty \leq C\left(|\eta| + \|f\|_\infty \right),$$

where $\overline{M} = \begin{pmatrix} 1 & -C \\ -C & 1 \end{pmatrix}$. Assuming $C < 1$ in $\overline{M}$, then, $\overline{M}$ is a nonsingular bounded M-matrix. Furthermore, we have $\overline{M}^{-1} > 0$, which completes the proof of the lemma. □

Lemma 3.2. *If $\mathbf{u}(t)$ is the solution of (1), then the truncation error*

$$|R_{r,i}| \le Ch_i,\ r = 1,2,\ \ i = 1,\dots,N.$$

Proof. For any $u_r(t)$ we now derive the truncation error $R^1_{r,i}$ and $R^2_{r,i}$ for the backward Euler scheme and the composite rectangular scheme respectively.

$$\begin{aligned} |R^1_{r,i}| &= \varepsilon_r |(u'_r - D^- u_r)(t_i)| \\ &\le C\varepsilon_1 (t_i - t_{i-1}) \max_{t\in[t_{i-1},t_i]} |u''_1(t)| \\ &\le C\varepsilon_1 N^{-1} \max_{t\in[t_{i-1},t_i]} (1+\varepsilon_1^{-1} e^{-\alpha t/\varepsilon_1}) \le CN^{-1} = Ch_i. \end{aligned} \tag{19}$$

Again,

$$\begin{aligned} |R^2_{r,i}| &= \left| \sum_{w=1}^{2} \sum_{j=0}^{i-1} \mathcal{K}_{rw}(t_i,t_j) U^N_{wj} - \sum_{w=1}^{2} \int_0^t \mathcal{K}_{rw} u_r(s)ds \right| \\ &\le \sum_{j=1}^{i-1} \frac{1}{2} (u'(\xi_1), u'(\xi_2))(t_i - t_{i-1})^2 \\ &\le \sum_{j=1}^{i-1} \frac{M_1 M_2}{2} h_i^2 \le CNh_i^2 \le Ch_i. \end{aligned} \tag{20}$$

Since $\mathbf{u} \in \mathscr{C}^{(1)}(0,1)$, there exist $M_1 > 0$ and $M_2 > 0$ such that $|u'(\xi_1)| \le M_1$ and $|u'(\xi_2)| \le M_2$ for all $\xi_1, \xi_2 \in (0,1)$. Combining the bounds obtained in (19) and (20), we get the desired results. □

Let $\mathbf{E} = \mathbf{u} - \mathbf{U}$ denotes the error of the finite difference scheme, such that

$$\begin{aligned} (L^N_r \mathbf{E})_i &= (L^N_r u_r)_i - (L^N_r U^N_r)_i = (L^N_r u_r)_i - f_r(t_i) \\ &= \varepsilon_r (D^- u_r - u'_r)_i + \left(\sum_{w=1}^{2} \sum_{j=0}^{i-1} \mathcal{K}_{rw}(t_i,t_j) U^N_{wj} h_j - \sum_{w=1}^{2} \int_0^t \mathcal{K}_{rw} u_r(s)ds \right) \end{aligned}$$

Theorem 3.3. *Consider $\mathbf{u}$ to be the solution of (1) and $\mathbf{U}$ being the numerical solution of (11). Then the following ε uniform estimate holds:*

$$\|\mathbf{u} - \mathbf{U}\|_\infty \le \begin{cases} CN^{-1}\ln N, & \text{on } S \text{ mesh}, \\ CN^{-1}, & \text{on } B\text{-}S \text{ mesh}. \end{cases}$$

Proof. Using Lemma 3.2, we know that

$$|R^j_{r,i}| \le Ch_i,\ \ r = 1,2,\ \ j = 1,2.$$

For the inner layer region, i.e., $[0,\tau_{\varepsilon_1}],[\tau_{\varepsilon_1},\tau_{\varepsilon_2}]$, we have $h_i = \frac{4\tau_{\varepsilon_1}}{N}$ and $\frac{4(\tau_{\varepsilon_1}-\tau_{\varepsilon_2})}{N}$ respectively. Also, $\tau_{\varepsilon_2} = \frac{2\varepsilon_2}{\alpha}\ln N$ and $\tau_{\varepsilon_1} < \frac{\tau_{\varepsilon_2}}{2}$. Now we calculate the bounds on each of the sub-intervals separately. So, $\tau_{\varepsilon_2} = \alpha^{-1}\varepsilon_2 \ln N$ and $\alpha^{-1}\varepsilon_2\ln N < \frac{1}{2}$. On the fine S-mesh, containing boundary layers, inequality (19) reduces to

$$\begin{aligned}
|R^1_{2,i}| &\le C\varepsilon_2 N^{-1} \max_{t\in[t_{i-1},t_i]}(1+\varepsilon_2^{-1}e^{-\alpha t/\varepsilon_2})\\
&\le C\varepsilon_2^{-1}\frac{4\alpha^{-1}\varepsilon_2\ln N}{N} \le CN^{-1}\ln N.
\end{aligned}$$

Now, on the B-S mesh, using Lemma 3.1, we can obtain $|R^1_{2,i}| \le CN^{-1}$. Similarly, for bound of the integral part,

$$\begin{aligned}
|R^2_{2,i}| &\le CN^{-1}\ln N, \text{ S-mesh}\\
|R^2_{2,i}| &\le CN^{-1}, \text{ B-Smesh}
\end{aligned}$$

Now, considering the outer layer region , i.e., $[\tau_{\varepsilon_2},1]$, for both the S mesh and B-S mesh, we know $t_i = \alpha^{-1}\varepsilon_2\ln N + \left(i-\frac{N}{2}\right)\frac{2(1-\tau_{\varepsilon_2})}{N}$, so, we can write for $H = \frac{2(1-\tau_{\varepsilon_2})}{N}$, hence the proof in the outer layer region for obtaining the bounds reamin same for both the type of meshes.

$$e^{-\frac{\alpha t_{i-1}}{\varepsilon_2}} - e^{-\frac{\alpha t_i}{\varepsilon_2}} = \frac{1}{N}e^{-\frac{\alpha\left(i-1-\frac{N}{2}\right)H_i}{\varepsilon_2}}\left(1-e^{-\frac{\alpha H}{\varepsilon}}\right) < N^{-1}.$$

From the above estimate, one can deduce that for the outer layer, $|R^j_{2,i}| \le CN^{-1},\ j=1,2$. Following the proceedings done above, we get the bounds for $R^j_{1,i},\ j=1,2$. Using the bounds obtained for both the layers and the result of Lemma 3.1, the proof of the theorem is done. □

4. Richardson extrapolation

The Richardson extrapolation is a well known acceleration technique used for improving the order of accuracy. In the technique, the solution is calculated on two different nested meshes and then after eliminating the leading error terms, desired higher order accuracy is obtained. One may refer to [12, 17] for detailed explanation.

In this paper, we applied the technique for enhancing the convergence rate to second order. Initially, we solved (1) with N mesh intervals. Keeping the transition parameters τ_{ε_1} and τ_{ε_2} intact, further, we solve it with $2N$ number of sub-intervals. Both the meshes are nested in such a way that $\Omega_N \subset \Omega_{2N}$. The solution on Ω_N is represented by $\mathbf{U}^N$ while on Ω_{2N}, the solution is represented using $\mathbf{U}^{2N}$. Thus from [17], we can write that

$$\begin{aligned}
(\mathbf{u}_i - \mathbf{U}^N_i) &= CN^{-1}\ln N + o(N^{-1}\ln N), \text{ for all } t_i\in\Omega_N\\
&= CN^{-1}\left(\frac{\alpha\tau_{\varepsilon_2}}{\varepsilon_2}\right) + o(N^{-1}\ln N) \qquad (21)
\end{aligned}$$

where $R^N(t_i)$ is $o(N^{-1}\ln N)$. In a similar manner, we have

$$(\mathbf{u}_i - \mathbf{U}_i^{2N}) = C(2N)^{-1}\left(\frac{\alpha\tau_{\varepsilon_2}}{\varepsilon_2}\right) + o(N^{-1}\ln N), \text{ for all } t_i \in \Omega_{2N}. \tag{22}$$

Terminating $O(N^{-1})$ terms from (21) and (22), we get

$$\mathbf{u}(t_i) - (2\mathbf{U}_i^{2N} - \mathbf{U}_i^N) = o(N^{-1}\ln N), \text{ for all } t_i \in \Omega_N.$$

Finally, we get the extrapolated solution as $\widetilde{U}_i$ denoted by,

$$\widetilde{U}_i = 2\mathbf{U}_i^{2N} - \mathbf{U}_i^N, \text{ for all } t_i \in \Omega_N. \tag{23}$$

Consider the error function as $\widetilde{\mathbf{E}} = \mathbf{u} - \widetilde{U}$ after extrapolation. Then, we define $\widetilde{\mathbf{E}}$ to be the solution for $r = 1,2$ and $i = 1,2,\ldots,N$ as

$$(L_r^N\widetilde{\mathbf{E}})_i = (L_r^N\mathbf{u})_i - (L_r^N\widetilde{U})_i, \ (\widetilde{\mathbf{E}}_r)_0 = 0.$$

Theorem 4.1. *Let* $\mathbf{u}$ *be the solution of (1) and* $\widetilde{U}$ *be the extrapolated solution obtained through Richardson extrapolation formula (23). Then we have the following* ε*-uniform estimate*

$$\|\mathbf{u} - \mathbf{U}\|_\infty \leq \begin{cases} CN^{-2}\ln^2 N, & \textit{on S mesh}, \\ CN^{-2}, & \textit{on B-S mesh}. \end{cases}$$

Proof. Here, we provide the proof of the theorem separately for inner layer and outer layer region. From Theorem 3.3, and applying the Taylor's series with integral form of the remainder, we have

$$\begin{aligned}
&\left|L_r^N(U_i - u_i) - L_r^N\widetilde{\mathbf{E}}_i\right| \\
&\leq \frac{\varepsilon_r}{2h_i}\left|\int_{t_{i-1}}^{t_i}(s-t_{i-1})^2 u_r'''(s)ds\right| + \left|\sum_{w=1}^{2}\sum_{j=0}^{i-1}\int_{t_{j-1}}^{t_j}\int_{t_{j-1}}^{t}[\mathcal{K}_{rw}(t_i,s)u_r(s)]''(s-t_{j-1})dsdt\right| \\
&\leq \frac{C}{2h_i}\int_{t_{i-1}}^{t_i}(t-t_{i-1})^2[1+|u_r'(s)|+|u_r''(s)|]ds \\
&\qquad + C\sum_{w=1}^{2}\sum_{j=0}^{i-1}\int_{t_{j-1}}^{t_j}\int_{t_{j-1}}^{t}\left[1+|u_r'(s)|+|u_r''(s)|\right](s-t_{j-1})dsdt \\
&\leq Ch_i^{-2} + C\int_{t_{i-1}}^{t_i}(s-t_{i-1})|u_r''(t)|ds + Ch_i^{-2} \leq Ch_i^2
\end{aligned}$$

Similarly, by using Taylor series expansion, we obtain

$$
\begin{aligned}
&\left| L_r^N (U_i^{2N} - u_i) - \frac{1}{2} L_r^N \widetilde{\mathbf{E}}_i \right| \\
&\leq \left| \frac{\varepsilon_r}{h_i} \int_{t_{i-1/2}}^{t_i} u_r'''(s)(s - t_{i-1/2})^2 ds \right| + \frac{1}{2} \sum_{w=1}^{2} \sum_{j=0}^{i-1} \left| \int_{t_{j-1}}^{t_j} \int_{t_{j-1}}^{t} (\mathcal{K}_{rw}(t_i, s) u_r(s))''(s - t_{j-1}) ds dt \right| \\
&\qquad + \frac{1}{2} \sum_{w=1}^{2} \sum_{j=0}^{i-1} \left| \int_{t_{j-1}}^{t_j} \int_{t_{j-1}}^{t} (\mathcal{K}_{rw}(t_i, s) u_r(s))''(t - s) ds dt \right| \\
&\leq C \int_{t_{j-1}}^{t_j} (s - t_{i-1}) \left[1 + |u_r'(s)| + |u_r''(s)| \right] ds \\
&\qquad + C \sum_{w=1}^{2} \sum_{j=0}^{i-1} \left| \int_{t_{j-1}}^{t_j} \int_{t_{j-1}}^{t} \left[1 + |u_r'(s)| + |u_r''(s)| \right] (s - t_{j-1}) ds dt \right| \\
&\leq C h_i^2.
\end{aligned}
$$

Combining the above two inequalities for obtaining the global error in the inner layer region with $h_i = 4\varepsilon_2 N^{-1} \ln N \alpha^{-1}$, we have,

$$
\begin{aligned}
\|\widetilde{U} - \mathbf{u}\|_\infty &\leq C \left| L^N \widetilde{U}_i - L^N \mathbf{u}_i \right| \\
&= C \left| \left[L^N (\mathbf{U}_i^{2N} - \mathbf{u}_i) - \frac{1}{2} L^N \widetilde{\mathbf{E}}_i \right] - \left[L^N (\mathbf{U}_i^N - \mathbf{u}_i) - L^N \widetilde{\mathbf{E}}_i \right] \right| \\
&\leq C \left| \left[L^N (\mathbf{U}_i^{2N} - \mathbf{u}_i) - \frac{1}{2} L^N \widetilde{\mathbf{E}}_i \right] \right| + \left| \left[L^N (\mathbf{U}_i^N - \mathbf{u}_i) - L^N \widetilde{\mathbf{E}}_i \right] \right| \\
&\leq C N^{-2} \ln^2 N, \text{ on the S mesh.}
\end{aligned} \tag{24}
$$

Using the Lemma 3.1, one can get the bounds on B-S mesh as $\|\widetilde{U} - \mathbf{u}\|_\infty \leq CN^{-2}$. The bounds on both the S mesh and B-S mesh are same in the outer layer region $[\tau_{\varepsilon_2}, 1]$ with $h_i = 2N^{-1}$ as follows:

$$
\begin{aligned}
\|\widetilde{U} - \mathbf{u}\|_\infty &\leq C \left| L^N \widetilde{U}_i - L^N \mathbf{u}_i \right| \\
&= C \left| \left[L^N (\mathbf{U}_i^{2N} - \mathbf{u}_i) - \frac{1}{2} L^N \widetilde{\mathbf{E}}_i \right] - \left[L^N (\mathbf{U}_i^N - \mathbf{u}_i) - L^N \widetilde{\mathbf{E}}_i \right] \right| \\
&\leq C \left| \left[L^N (\mathbf{U}_i^{2N} - \mathbf{u}_i) - \frac{1}{2} L^N \widetilde{\mathbf{E}}_i \right] \right| + \left| \left[L^N (\mathbf{U}_i^N - \mathbf{u}_i) - L^N \widetilde{\mathbf{E}}_i \right] \right| \\
&\leq C N^{-2}.
\end{aligned} \tag{25}
$$

Combining (24), (25), and estimate from Lemma 3.1 we get the desired result. □

5. Numerical simulation

To demonstrate that the numerical results reproduce the error estimates, we have performed a few numerical experiments.

Example 5.1. *The following system of SPVIDEs is considered*

$$\varepsilon_1 u_1' + (2+t)u_1 - u_2 + \int_0^t (u_1^2 + u_2^2) ds = 1 - t,$$
$$\varepsilon_2 u_2' - (1+t)u_1 + (2+t)u_2 + \int_0^t (u_1^2 u_2^2) ds = t,$$
$$u_1(0) = 1, \quad u_2(0) = 0.$$

Example 5.2. *Consider the system*

$$\varepsilon_1 u_1' + (2+\tan(t))u_1 - 2tu_2 + \int_0^t ((t+s)e^{u_1} + e^{tsu_2}) ds = t^2,$$
$$\varepsilon_2 u_2' - t\sin(t)u_1 + e^t u_2 + \int_0^t (tu_1(s) + s^2 u_2) ds = \sin(t),$$
$$u_1(0) = 2, \quad u_2(0) = 2.$$

The exact solution of above examples are unknown. So, we use the double mesh principle to obtain the maximum point-wise errors and order of convergence. For any given N, the maximum point-wise error is calculated by using $\Sigma_\varepsilon^N = \|\mathbf{U}^N - \mathbf{U}^{2N}\|_\infty$. The order of accuracy is evaluated as: $r_\varepsilon^N = \log_2\left(\frac{\Sigma_\varepsilon^N}{\Sigma_\varepsilon^{2N}}\right)$. Figure 1(a) shows the solution plots for both the solutions u_1 and u_2 with different values of ε. The stiffness in the layers can be clearly observed from the graphs as the perturbation factor reduces. Figure 1(b) depicts the total error curve before and after extrapolation for $\varepsilon_1 = 10^{-3}$ and $\varepsilon_2 = 10^{-2}$. The picture describes the effect on point-wise errors after the post-processing technique. The Log-log plots are also demonstrated for the examples. Figure 2(a) draws the error obtained for u_2 at $\varepsilon_1 = \varepsilon_2 = 10^{-2}$ on a logarithmic scale. Similarly, Figure 2(b) depicts the log-log plots for u_1 at $\varepsilon_1 = 10^{-6}$ and $\varepsilon_2 = 10^{-3}$. The computed errors drop at about the same rate as those shown theoretically, and the rate is doubled after the application of Richardson extrapolation.

Tabular data are also recorded for showing the correctness and effectiveness of the proposed scheme. Tables 1 and 2 show the maximum point-wise errors and rate of convergence before and after extrapolation keeping ε_2 fixed and with varying ε_1. It can be observed that the scheme attains ε-uniform convergence before and after extrapolation and the convergence rate is doubled after the use of extrapolation formula. In the similar way, Tables 3 and 4 record the Σ_ε^N and r_ε^N for Example 5.2. One can observe that though we have assumed $0 < \varepsilon_1 \leq \varepsilon_2 \ll 1$ theoretically, but computationally the proposed scheme gives accurate results even if the assumed condition is little violated. Finally, we have computed the results on both the S mesh and B-S mesh in Table 5 which shows that B-S mesh gives greater accuracy than S mesh before and after extrapolation.

6. Conclusion

In this paper, the Richardson extrapolation technique is used on the classical finite difference scheme for solving a system of Volterra integro-differential equations exhibiting boundary layers. First, by using an upwind scheme for the derivative component, and rectangular rule for the non-linear integral part, a difference scheme is constructed on the non-uniform meshes. Error analysis is carried out and first order accuracy is attained. Then, the Richardson extrapolation is used on the proposed scheme, successfully improving the order of accuracy from first order to second order. Finally, the theoretical observations are substantiated through parameter-uniform error estimates and are corroborated by various numerical tests.

Disclosure statement

The authors declare that they have no conflicts of interest.

Acknowledgements

None

Funding

This research did not receive any specific grant from funding agencies in the public, commercial, or not-for-profit sectors.

References

[1] M.I. Berenguer, A.I. Garralda-Guillem, and M.R. Galán, *An approximation method for solving systems of Volterra integro-differential equations*, Appl. Numer. Math., 67 (2013), 126-135.

[2] A.M. Bijura, *Singularly perturbed Volterra integro-differential equations*, Quaest. Math., 25 (2002), 229-248.

[3] A. Ebadian and A.A. Khajehnasiri, *Block-pulse functions and their applications to solving systems of higher-order nonlinear Volterra integro-differential equations*, Electron. J. Differ. Equ., 54 (2014), 1-9.

[4] J. Huang, Z. Cen, A. Xu, and L.B. Liu, *A posteriori error estimation for a singularly perturbed Volterra integro-differential equation*, Numer. Algorithms 83 (2020), 549–563.

[5] B.C. Iragi and J.B. Munyakazi, *A uniformly convergent numerical method for a singularly perturbed Volterra integro-differential equation*, Int. J. Comput. Math., 97 (2020), 759-771.

[6] I.A. Irwaq, M. Alquran, M. Ali, I. Jaradat, and M.S.M. Noorani, *Attractive new fractional-integer power series method for solving singularly perturbed differential equations involving mixed fractional and integer derivatives*, Results Phys., 20 (2021), 103780.

[7] J.P. Kauthen, *Implicit Runge-Kutta methods for singularly perturbed integro-differential systems*, Appl. Numer. Math., 18 (1995), 201-210.

[8] S. Kumar and M. Kumar, *Parameter-robust numerical method for a system of singularly perturbed initial value problems*, Numer. Algorithms, 59 (2012), 185-195.

[9] H. Liang and H. Brunner, *Collocation methods for integro-differential algebraic equations with index 1*, IMA J. Numer. Anal., 40 (2020), 850-885.

[10] Y. Liang, L.B. Liu, and Z. Cen, *A posteriori error estimation in maximum norm for a system of singularly perturbed Volterra integro-differential equations*, Comput. Appl. Math., 39 (2020), 1-17.

[11] J. Mohapatra and L. Govindarao, *A fourth-order optimal numerical approximation and its convergence for singularly perturbed time delayed parabolic problems*, Iranian Journal of Numerical Analysis and Optimization, 12 (2022), 250-276.

[12] A. Panda, J. Mohapatra, and I. Amirali, *A second-order post-processing technique for singularly perturbed Volterra integro-differential equations*, Mediterr. J. Math., 18 (2021), 1-25.

[13] J. Rashidinia and A. Tahmasebi, *Systems of nonlinear Volterra integro-differential equations*, Numer. Algorithms, 59 (2012), 197-212.

[14] K.S. Sankar and L.J.T. Doss, *On parameter uniform and layer resolving numerical method for a singularly perturbed model in aerodynamics*, Results in Control and Optimization, 10 (2023), 100208.

Submitted to Journal of Integral Equations and Applications - NOT THE PUBLISHED VERSION

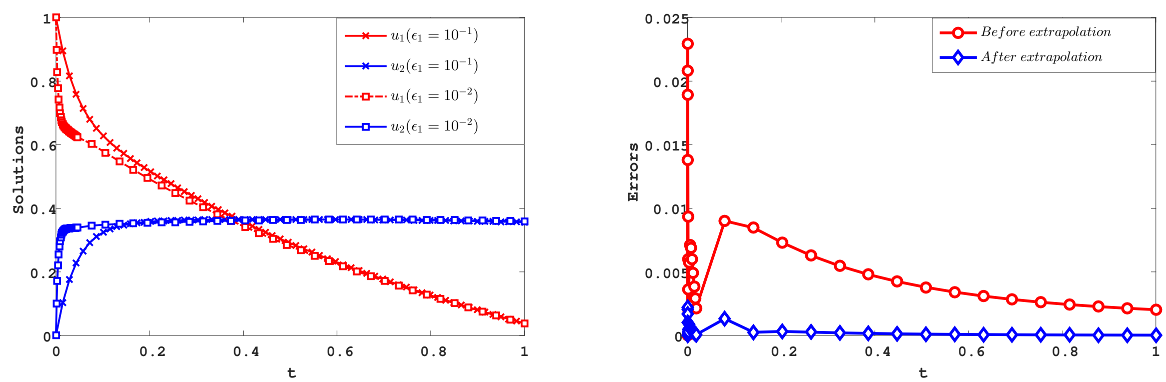

(a) Example 5.1 *(b) Example 5.2*

FIGURE 1. Solution and error plots

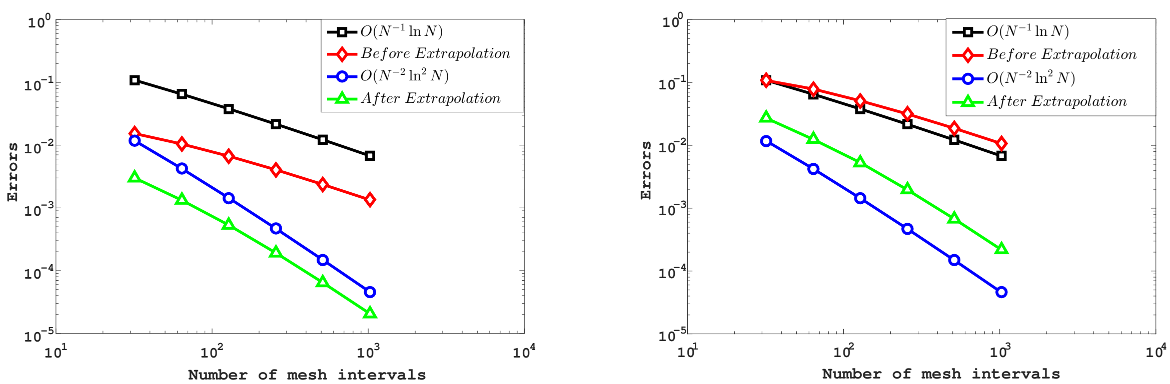

(a) Example 5.1 *(b) Example 5.2*

FIGURE 2. Log-log plots

[15] S. Sevgin, *Numerical solution of a singularly perturbed Volterra integro-differential equation*, Adv. Differ. Equ., 2014 (2014), 1-15.

[16] D. Shakti and J. Mohapatra, *Parameter-uniform numerical methods for a class of parameterized singular perturbation problems*, Numer. Anal. Appl., 12 (2019), 176-190.

[17] M.K. Singh and S. Natesan, *Richardson extrapolation technique for singularly perturbed system of parabolic partial differential equations with exponential boundary layers*, Appl. Math. Comp., 333 (2018), 254-275.

[18] Ö. Yapman, G.M. Amiraliyev, and I. Amirali, *Convergence analysis of fitted numerical method for a singularly perturbed non-linear Volterra integro-differential equation with delay*, J. Comput. Appl. Math., 355 (2019), 301-309.

[19] V. Vougalter and V. Volpert, *On the solvability of some systems of integro-differential equations with concentrated sources*, Z. Angew. Math. Phys., 73 (2022), 252.

[20] H.R. Wilson and J.D. Cowan, *Evolution of the Wilson-Cowan equations*, Biol. Cybernet., 115 (2021), 643-653.

TABLE 1. Σ_ε^N and r_ε^N before and after extrapolation for Example 5.1 for $\varepsilon_2 = 10^{-1}$ for u_1.

ε_1	N	32	64	128	256	512	1024
10^{-1}	Before	9.4414e-3	6.3316e-3	3.9590e-3	2.3620e-3	1.3642e-3	7.6958e-4
	rate	0.576	0.677	0.745	0.792	0.826	
	After	1.3600e-3	5.8153e-4	2.2251e-4	7.7772e-5	2.5663e-5	8.1087e-6
	rate	1.226	1.386	1.517	1.600	1.662	
10^{-2}	Before	2.0528e-2	1.3869e-2	8.7787e-3	5.2945e-3	3.0775e-3	1.7432e-3
	rate	0.566	0.660	0.730	0.783	0.820	
	After	3.6162e-3	1.6163e-3	6.3052e-4	2.2453e-4	7.5154e-5	2.3979e-5
	rate	1.162	1.358	1.490	1.579	1.648	
10^{-4}	Before	2.0713e-2	1.3916e-2	8.7879e-3	5.2791e-3	3.0685e-3	1.7369e-3
	rate	0.574	0.663	0.735	0.783	0.821	
	After	3.5063e-3	1.5689e-3	6.0852e-4	2.1667e-4	7.2479e-5	2.3074e-5
	rate	1.160	1.366	1.490	1.580	1.651	
10^{-5}	Before	2.0714e-2	1.3916e-2	8.7875e-3	5.2787e-3	3.0683e-3	1.7368e-3
	rate	0.574	0.663	0.735	0.783	0.821	
	After	3.5053e-3	1.5685e-3	6.0832e-4	2.1660e-4	7.2455e-5	2.3066e-5
	rate	1.160	1.366	1.490	1.580	1.651	
10^{-6}	Before	2.0714e-2	1.3916e-2	8.7875e-3	5.2787e-3	3.0683e-3	1.7368e-3
	rate	0.574	0.663	0.735	0.783	0.821	
	After	3.5053e-3	1.5685e-3	6.0832e-4	2.1660e-4	7.2455e-5	2.3066e-5
	rate	1.160	1.366	1.490	1.580	1.651	

DEPARTMENT OF APPLIED MATHEMATICS AND COMPUTING, ITER, SIKSHA 'O' ANUSANDHAN UNIVERSITY, BHUBANESWAR, INDIA.
Email address: 519MA2004@nitrkl.ac.in

DEPARTMENT OF MATHEMATICS, NATIONAL INSTITUTE OF TECHNOLOGY ROURKELA, INDIA.
Email address: jugal@nitrkl.ac.in.

TABLE 2. Σ_ε^N and r_ε^N before and after extrapolation for Example 5.1 for $\varepsilon_2 = 10^{-1}$ for u_2.

ε_1	N	32	64	128	256	512	1024
10^{-1}	Before	5.8510e-3	3.6791e-3	2.2120e-3	1.2890e-3	7.3346e-4	4.1017e-4
	rate	0.669	0.734	0.779	0.814	0.838	
	After	5.6058e-4	2.2339e-4	8.1235e-5	2.7617e-5	8.9495e-6	2.8007e-6
	rate	1.327	1.459	1.557	1.626	1.676	
10^{-2}	Before	3.7919e-3	2.3063e-3	1.3428e-3	7.5704e-4	4.1699e-4	2.2578e-4
	rate	0.717	0.780	0.827	0.860	0.885	
	After	3.1042e-4	1.1908e-4	4.1301e-5	1.3402e-5	4.1390e-6	1.2345e-6
	rate	1.382	1.528	1.624	1.695	1.745	
10^{-4}	Before	5.2299e-3	3.3089e-3	1.9999e-3	1.1672e-3	6.6456e-4	3.7177e-4
	rate	0.660	0.726	0.777	0.813	0.838	
	After	5.3814e-4	2.1506e-4	7.8216e-5	2.6581e-5	8.6145e-6	2.6949e-6
	rate	1.323	1.459	1.557	1.626	1.677	
10^{-5}	Before	5.2459e-3	3.3208e-3	2.0076e-3	1.1722e-3	6.6760e-4	3.7360e-4
	rate	0.660	0.726	0.776	0.812	0.837	
	After	5.4066e-4	2.1624e-4	7.8678e-5	2.6748e-5	8.6729e-6	2.7143e-6
	rate	1.322	1.459	1.557	1.625	1.676	
10^{-6}	Before	5.2459e-3	3.3208e-3	2.0076e-3	1.1722e-3	6.6760e-4	3.7360e-4
	rate	0.660	0.726	0.776	0.812	0.837	
	After	5.4066e-4	2.1624e-4	7.8678e-5	2.6748e-5	8.6729e-6	2.7143e-6
	rate	1.322	1.459	1.557	1.625	1.676	

TABLE 3. Σ_{ε}^{N} and r_{ε}^{N} before and after extrapolation for Example 5.2 for $\varepsilon_2 = 10^{-3}$ for u_2.

ε_1	N	32	64	128	256	512	1024
10^{-1}	Before	3.8425e-2	2.4409e-2	1.4749e-2	8.6127e-3	4.9070e-3	2.7464e-3
	rate	0.655	0.727	0.776	0.812	0.837	
	After	3.3951e-3	1.4465e-3	4.4177e-4	1.4183e-4	4.5841e-5	1.4323e-5
	rate	1.231	1.711	1.639	1.629	1.678	
10^{-3}	Before	3.8425e-2	2.4409e-2	1.4749e-2	8.6127e-3	4.9070e-3	2.7464e-3
	rate	0.655	0.727	0.776	0.812	0.837	
	After	2.9527e-3	1.1603e-3	4.1874e-4	1.4173e-4	4.5809e-5	1.6417e-5
	rate	1.348	1.470	1.563	1.629	1.480	
10^{-4}	Before	4.4835e-2	2.7659e-2	1.5883e-2	8.7943e-3	4.7157e-3	2.4759e-3
	rate	0.697	0.800	0.853	0.899	0.929	
	After	5.2353e-3	2.0276e-3	7.0104e-4	2.2490e-4	6.7922e-5	1.9691e-5
	rate	1.369	1.532	1.640	1.727	1.786	
10^{-5}	Before	6.4202e-2	4.2716e-2	2.6327e-2	1.5572e-2	8.9107e-3	4.9841e-3
	rate	0.588	0.698	0.758	0.805	0.838	
	After	8.7957e-3	3.7437e-3	1.4337e-3	4.9758e-4	1.6275e-4	5.1072e-5
	rate	1.232	1.385	1.527	1.612	1.672	
10^{-7}	Before	6.7272e-2	4.5052e-2	2.8015e-2	1.6693e-2	9.6279e-3	5.4268e-3
	rate	0.578	0.685	0.747	0.794	0.827	
	After	9.2630e-3	3.9810e-3	1.5416e-3	5.3939e-4	1.7776e-4	5.6248e-5
	rate	1.218	1.369	1.515	1.601	1.660	
10^{-8}	Before	6.7272e-2	4.5052e-2	2.8015e-2	1.6693e-2	9.6279e-3	5.4268e-3
	rate	0.578	0.685	0.747	0.794	0.827	
	After	9.2630e-3	3.9810e-3	1.5416e-3	5.3939e-4	1.7776e-4	5.6248e-5
	rate	1.218	1.369	1.515	1.601	1.660	

TABLE 4. Σ_ε^N and r_ε^N before and after extrapolation for Example 5.2 for $\varepsilon_2 = 1$ for u_1.

ε_1	N	32	64	128	256	512	1024
10^0	Before	1.3152e-2	6.5504e-3	3.2693e-3	1.6332e-3	8.1627e-4	4.0805e-4
	rate	1.006	1.003	1.001	1.001	1.000	
	After	1.2877e-2	4.1626e-3	1.2045e-3	3.2607e-4	8.4691e-5	2.1597e-5
	rate	1.629	1.789	1.885	1.945	1.971	
10^{-1}	Before	7.3246e-2	4.2288e-2	2.3259e-2	1.2196e-2	6.2458e-3	3.1616e-3
	rate	0.793	0.862	0.931	0.965	0.982	
	After	1.2877e-2	4.1626e-3	1.2045e-3	3.2607e-4	8.4691e-5	2.1597e-5
	rate	1.629	1.789	1.885	1.945	1.971	
10^{-2}	Before	1.0645e-1	7.7840e-2	5.0578e-2	3.1224e-2	1.8455e-2	1.0556e-2
	rate	0.452	0.622	0.696	0.759	0.806	
	After	2.6737e-2	1.2281e-2	5.2461e-3	1.9410e-3	6.6711e-4	2.1613e-4
	rate	1.122	1.227	1.434	1.541	1.626	
10^{-4}	Before	1.0758e-1	7.8671e-2	5.1113e-2	3.1556e-2	1.8650e-2	1.0667e-2
	rate	0.452	0.622	0.696	0.759	0.806	
	After	2.7013e-2	1.2413e-2	5.3022e-3	1.9616e-3	6.7433e-4	2.1847e-4
	rate	1.122	1.227	1.435	1.540	1.626	
10^{-5}	Before	1.0758e-1	7.8671e-2	5.1113e-2	3.1556e-2	1.8650e-2	1.0667e-2
	rate	0.452	0.622	0.696	0.759	0.806	
	After	2.7013e-2	1.2413e-2	5.3022e-3	1.9616e-3	6.7433e-4	2.1847e-4
	rate	1.122	1.227	1.435	1.540	1.626	

TABLE 5. Σ_{ε}^{N} and r_{ε}^{N} before extrapolation for Example 5.2 for $\varepsilon_2 = 1e-1$ for u_1.

ε_1		S mesh 64	128	256	B-S mesh 64	128	256
$1e-1$	Before	3.5980e-3	2.1427e-3	1.2375e-3	3.0571e-3	1.4614e-3	8.1541e-4
	rate	0.745	0.792	0.813	0.991	1.065	1.101
	After	1.8667e-3	5.9148e-4	1.6986e-4	1.2342e-3	3.1903e-4	8.1002e-5
	rate	1.413	1.658	1.800	1.952	1.978	1.988
$1e-5$	Before	3.6054e-3	2.1469e-3	1.2399e-3	3.3480e-3	1.7304e-3	8.7855e-4
	rate	0.680	0.748	0.792	0.927	0.952	0.978
	After	3.4867e-4	1.4898e-4	5.5247e-5	2.9889e-4	8.4898e-5	2.2334e-5
	rate	1.227	1.431	1.550	1.816	1.926	1.998
$1e-7$	Before	3.6054e-3	2.1469e-3	1.2399e-3	3.3480e-3	1.7304e-3	8.7855e-4
	rate	0.680	0.748	0.792	0.927	0.952	0.978
	After	3.4867e-4	1.4898e-4	5.5247e-5	2.9889e-4	8.4898e-5	2.2334e-5
	rate	1.227	1.431	1.550	1.816	1.926	1.998